Influence of Nanoparticle Properties on Non-Photochemical Laser-Induced Nucleation

Cui, Pingping; Korede, Vikram; van Tooren, Rohan P.Y.; Nagalingam, Nagaraj; Wang, Runze; Yin, Qiuxiang; van der Heijden, Antoine E.D.M.; Kramer, Herman J.M.; Eral, Hüseyin Burak

DOI
10.1021/acs.cgd.5c01080

Publication date
2026

Document Version
Final published version

Published in
Crystal Growth and Design

Citation (APA)
Cui, P., Korede, V., van Tooren, R. P. Y., Nagalingam, N., Wang, R., Yin, Q., van der Heijden, A. E. D. M., Kramer, H. J. M., & Eral, H. B. (2026). Influence of Nanoparticle Properties on Non-Photochemical Laser-Induced Nucleation. *Crystal Growth and Design*, *26*(1), 144-154. https://doi.org/10.1021/acs.cgd.5c01080

CRYSTAL GROWTH & DESIGN

pubs.acs.org/crystal

Article

Influence of Nanoparticle Properties on Non-Photochemical Laser-Induced Nucleation

Pingping Cui,[‖] Vikram Korede,[‖] Rohan P. Y. van Tooren,[‖] Nagaraj Nagalingam, Runze Wang, Qiuxiang Yin, Antoine E. D. M. van der Heijden, Herman J. M. Kramer, and Hüseyin Burak Eral*

Cite This: *Cryst. Growth Des.* 2026, 26, 144−154

Read Online

ACCESS | Metrics & More | Article Recommendations | Supporting Information

ABSTRACT: In nonphotochemical laser-induced nucleation (NPLIN), an unfocused nanosecond laser pulse with low intensity (≈MW/cm^2) triggers nearly instantaneous nucleation in supersaturated solutions, a process that would typically take days or weeks when the solution is left undisturbed. Previous studies have shown that the introduction of nanoparticles into supersaturated solutions enhances the probability of NPLIN measured during a fixed time window, compared to undoped control experiments. However, the precise mechanisms driving this enhancement remain unclear hampering industrial implementation of NPLIN. In this study, we systematically investigate how the properties of doped nanoparticles—specifically their concentration and chemical composition—affect the NPLIN probability in supersaturated urea solutions. We observed that higher laser intensities resulted in elevated NPLIN probabilities at a fixed pegylated gold nanoparticle (AuNP) concentration and supersaturation, while increasing concentrations of AuNPs at a fixed laser intensity and supersaturation interestingly led to higher NPLIN probabilities. Moreover, supersaturated solutions doped with gold nanoparticles exhibited significantly higher NPLIN probabilities compared to silica nanoparticle doped solutions at comparable nanoparticle size and concentration. We interpret these experimental results based on the impurity heating hypothesis as well as recent results highlighting the role of thermocavitation. We furthermore propose a helicopter-view model based on a thermodynamic equilibrium stage sequence. Our findings highlight the significance of nanoparticle properties in the design of heteronucleants optimized for NPLIN applications.

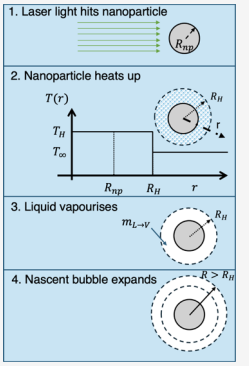

1. INTRODUCTION

Nonphotochemical laser-induced nucleation (NPLIN) employs nanosecond laser pulses to initiate nucleation in supersaturated solutions without causing any detectable photochemical reaction, as neither the solute nor the solvent molecules absorb light at the irradiated wavelength.[1−3] Since its serendipitous discovery by Garetz et al. in 1996 using urea,[4] NPLIN has been applied to crystallize over 50 distinct compounds, including small organic molecules,[5] cocrystals,[6] proteins and inorganic salts.[7] NPLIN reduces the induction time for supersaturated solutions from weeks to mere minutes or seconds.[8,9] Moreover, NPLIN has been reported to offer control over crystal morphology[10] and (pseudo)polymorphic forms[11,12] although contradicting reports exist on this topic[11,13,14] as well as reports with other laser irradiation parameters.[15,16] More recently, NPLIN has also been used for cocrystal crystallization.[6] Despite these advances experimentally[17,18] and theoretically,[19,20] a comprehensive physical understanding of NPLIN remains elusive as summarized in recent reviews.[1,7]

Initial studies of NPLIN attributed the observed enhanced nucleation rates to the interaction between the laser electric field and the dipole moment of the solute molecules, according to the optical Kerr effect (OKE).[4] This hypothesis suggests that the electric field of pulsed laser light induces anisotropic polarization, producing a weak torque that aligns the most polarizable axis of the molecule in the direction of the applied electric field. Furthermore, for aqueous glycine solutions, it was observed that the linear and circular polarization of light produced a different electric field, which altered the structural motifs of the crystal formed.[13] Subsequent studies, however, have shown that the orientation of the crystal does not depend on the direction of the electric field.[14]

In conflict with earlier reports, recent studies did not observe a definitive correlation between glycine polymorphism[21] and laser polarization.[11,22] Interestingly, Irimia et al. reported that the polymorphic form that crystallizes from the solution with NPLIN was different from that that nucleates during flash cooling.[11] This result might allow one to speculate that light irradiation could influence the polymorphism but via a different pathway than suggested in previous reports.[13] Monte Carlo simulations suggest that the intensities of the lasers used in the experiments are too low to induce nucleation

Received: July 24, 2025
Revised: December 9, 2025
Accepted: December 9, 2025
Published: December 23, 2025

via orientational bias.[23] As a result, an alternative mechanism, dielectric polarization (DP), has been proposed.[24] This mechanism considers the isotropic electronic polarizability of molecular clusters. According to this theory, the optical electric field could decrease the free energy within the clusters due to the difference in the dielectric permittivity between the solute and the solvent,[7] thus reducing the size of the critical nucleus required for nucleation.[24] Although the DP model has been successful in correlating nucleation probability with peak laser intensity and solution supersaturation, it fails to explain the influence of laser pulse duration and threshold intensity on nucleation. Knott et al.[25] demonstrated that while a laser could induce CO_2 bubble nucleation in carbonated water, this phenomenon could not be adequately explained by the DP mechanism.

Interestingly, the nucleation probability in filtered solutions—such as those of glycine, NH_4Cl, and KCl—was lower than in unfiltered solutions under identical laser irradiation conditions, highlighting the significant role of insoluble impurity nanoparticles or clusters in NPLIN.[11,26,27] This effect could be reversed by adding iron-oxide (Fe_3O_4) nanoparticles to filtered NH_4Cl samples, as shown by Ward et al.,[27] leading to the proposal of a third NPLIN mechanism: nanoparticle heating. This mechanism suggests that laser-absorbing nanoparticles heat up, causing local vaporization and bubble formation. It is hypothesized that evaporation of the solvent near these transient bubbles increases local supersaturation, facilitating nucleation.

Although experimental efforts to directly visualize such bubbles in NPLIN experiments (unfocused beam hence ≈ MW/cm^2 laser flux) had previously failed, Hidman et al.,[28] building on experimental results from Soare et al.[29] with focused irradiation (≈GW/cm^2 flux), developed a finite element simulation framework that supported the plausibility of solvent evaporation around an nanoparticle impurity. However, in the absence of dedicated experiments, their findings remained theoretical. This gap was addressed by Nagalingam et al.,[19] who used high-speed video microscopy to record bubble expansion and collapse events followed by KCl crystallization. Their experiments, enabled by the addition of ppm-level $KMnO_4$ and a modified optical setup, were the first to provide experimental and theoretical verification of the thermocavitation hypothesis. Simulations in that study revealed short-lived supersaturation peaks (on the order of microseconds) at the vapor−liquid interface of a thermocaviations bubble during rapid bubble expansion. A key limitation of the Nagalingam et al. study, however, was the use of a focused laser beam; whether cavitation could occur under collimated beam conditions remained an open question until Barber and Alexander.[17] recently reported high speed microscopy images of cavitation with an unfocused laser. Despite these advances, the detailed interplay between laser parameters, impurity properties, and NPLIN behavior remains largely uncharted. On the topics of additives,[30−32] morphology[7,31] and polymorphism control[5,11] significant gaps in current understanding of NPLIN exist.

Further supporting the role of nanoparticle heating, Korede et al.[9] found that adding Fe_3O_4 nanoparticles to filtered KCl samples not only increased nucleation probability but also altered crystal morphology from cubic to needle-like in a microfluidic droplet system. Similarly, Briard et al.[33] explored how solid impurities influence NPLIN in aqueous ethylenediamine sulfate (EDS) solutions, further substantiating the heating-based mechanism. Currently, how laser−impurity interactions and the nanoparticle properties affect NPLIN behavior remain largely unexplored. More recently, Li et al. conducted a systematic study on the role of filtration, aging and doped impurity size.[30]

The primary objective of this study is to investigate the influence of nanoparticle properties (particularly concentration and chemical composition) on the NPLIN probability. Experiments were conducted using supersaturated urea solution (S = 1.5 at 25 °C) with polyethylene glycol stabilized gold nanoparticles (AuNPs) of various concentrations and silica nanoparticles at a laser wavelength of 532 nm. We observe that filtered solutions yielded lower NPLIN probability, while postfiltration doping with AuNPs restored it to levels higher than unfiltered undoped solutions—consistent with findings on iron oxide and other nanoparticles.[9,18,27,30] Increasing laser intensity also increased NPLIN probability across all solutions. Notably, AuNP doping produced a comparable effect to increased laser intensity, whereas silica nanoparticles resulted in significantly lower NPLIN probability under identical conditions of supersaturation, laser intensity, and particle concentration. We propose a scaling relation for the laser intensity dependence and outline a thermodynamic equilibrium-based model of thermocavitation. These results underscore the role of nanoparticle properties in NPLIN, suggesting that rational design of such heteronucleants may be essential for industrial applications.

2. EXPERIMENTAL SECTION

2.1. Materials and Method. Urea (molecular biology grade: 98.5−101.5%, CAS: 7447-40-7) and AuNPs dispersed in phosphate buffered saline (PBS) with 50 nm diameter (SKU 753645, 3.5 × 10^{10} NPs/ml), were procured from Sigma-Aldrich, Netherlands. Silica nanospheres with a diameter of 50 nm (10 mg/mL ≈ 7.64 × 10^{10} NPs/ml), dispersed in Milli-Q water, was obtained from Alpha Nanotech Inc. Thiol-functionalized methoxyl polyethylene glycol (PEG-SH) with a molecular weight of 5000 Da was obtained from Rapp Polymere GMBH, Germany. This PEG-SH was used to functionalize the gold nanoparticles. Silica nanoparticles were not functionalized.

Early in the study, we observed that colloidal stability of nanoparticles was critical in our experiments as nanoparticle aggregation alters the size and concentration of suspended nanoparticles over the course of the experiments. Sterically stabilized AuNPs were chosen as a result of their higher chemical and colloidal stability in concentrated urea solutions. Additionally, gold nanoparticles are known for their unique optical properties, particularly their strong absorption in the visible light spectrum, which is expected to enhance the laser−impurity interaction.[34]

Ultrapure water, from an internal Milli-Q system (ELGA Purelab, UK, 18.2 MΩ cm), was used in all experiments.

Urea solution (30.2 mol kg^{-1}, S = 1.5 at 25 °C) was prepared by dissolving urea in ultrapure water. This solution was placed in an ultrasonic heating water bath for 1 h, then transferred to an oven set at 50 °C overnight to ensure complete dissolution. The solution was then directly filtered into preheated 8 mL borosilicate glass vials using 0.22 μm (PTFE syringe filter). The vials were maintained at 50 °C during this process. For each experimental set, 100 samples were prepared. After filtration, the vials were transferred to a 50 °C water bath, gradually cooled to 25 °C in 3 h and aged for a day before laser exposure. Samples showing spontaneous nucleation prior to laser experiments were excluded from the study.

2.2. Filtered Solutions Doped with Nanoparticles. *2.2.1. Gold Nanoparticles.* Urea supersaturated solutions with different concentrations were prepared, doped with various concentrations of AuNPs to maintain a consistent supersaturation level (S = 1.5 at 25 °C). The manufacturer of nanoparticles reported

https://doi.org/10.1021/acs.cgd.5c01080
Cryst. Growth Des. 2026, 26, 144−154

their size as 50 nms. Nanoparticles are then added via a micropipette to this solution. The micropipette is preheated to 37 °C.

Detailed information on the specific concentrations of the urea solutions, the volume of the AuNPs suspension added, and the consequent concentrations of the AuNPs can be found in the Table 1.

Table 1. Summary of Urea Concentrations with Corresponding Volumes and Concentrations of Doped AuNPs

urea solution concentration (mol kg^{-1})	volume of AuNPs suspension added (ml)	concentration of AuNPs (particles/ml)
30.209	0.001	8.75×10^6
30.337	0.02	1.74×10^8
30.488	0.04	3.47×10^8
30.639	0.06	5.17×10^8
30.790	0.08	6.86×10^8
31.318	0.15	1.27×10^9

2.3. Laser Irradiation Experiments. Figure 1 depicts the schematic of the experimental setup that includes a Q-switched Nd/YAG laser (Continuum, Powerlite DLS8000), which emits 7 ns pulses of linearly polarized light with a wavelength of 532 nm at a frequency of 10 Hz. The direction of light was adjusted by a mirror (NB1−K13, Thorlabs) or a beam splitter (BSN10, Thorlabs), according to the desired intensity levels. Subsequently, the fundamental beam, with a diameter of 9 mm, was passed through a Galilean telescope, resulting in a decrease in its diameter to 4.5 mm. To eliminate any artifacts produced by the laser, an iris was used also with 4.5 mm diameter. Before irradiating the samples through its center, the average energy per pulse was determined by averaging the measurements from 20 pulses using an energy meter (QE25LP-H-MB-QED-D0, Gentec EO). Each sample, free from spontaneous nucleation, was subjected to a single pulse of laser light at various intensities (10, 50, 100, 200, and 376 MW/cm^2). Immediately following the laser exposure, the sample was returned to the water bath set at 25 °C. The presence of crystals in the vials was examined after 60 min. This period was chosen because of coherence with prior studies,[26] and also because in preliminary experiments both laser and control samples showed no further nucleation statistics changes after 30 min. The nucleation probability, denoted as $P(t_{obs} = 60\ min)$, was then calculated as the ratio of nucleated samples to the overall number of samples irradiated.

2.4. Dynamic Light Scattering Experiments. Dynamic light scattering (DLS) analysis were performed using a Zetasizer Pro (Malvern Panalytical Ltd., UK) to determine the particle size distribution (PSD) of filtered solution, unfiltered solution, and filtered urea solution doped with AuNPs. DLS measurements were conducted at 25 °C using a 633 nm wavelength laser diode at a scattering angle of 173°. The non-negative least-squares (NNLS) fitting algorithm was employed for calculating particle size distributions (PSD). To avoid urea crystallization during DLS tests, the solution concentration was kept at 16.65 mol kg^{-1} ($S = 0.98$). It is important to note that the PSD obtained from DLS represents the hydrodynamic diameter, which may not precisely correspond to the physical size of the nanoparticles observed in transmission electron microscopy.

3. RESULTS

3.1. Effect of Filtration and Doping. Laser-induced nucleation experiments were performed with supersaturated filtered urea solution ($S = 1.5$ at 25 °C) doped with PEG-coated AuNPs (50 nm nominal diameter, 6.86×10^8 NPs/ml), at an incident wavelength of 532 nm and peak intensity of 376 MW/cm^2 to determine if filtration and nanoparticle addition would alter NPLIN nucleation probability compared to control experiments. The nucleation probabilities obtained in these experiments are shown in the Figure 2A.

The unfiltered solution showed a nucleation probability of 22%, significantly higher than the 4% in filtered samples, highlighting the role of nanoimpurities/nanoclusters in NPLIN. The nature of these filtered nanoparticles or prenucleation clusters has been discussed and speculated extensively in the literature.[9,27] In a nutshell, these nanoscopic particles could be chemically (i) identical to solute/solvent molecules in the case of solute prenucleation clusters or (ii) distinct from the solute or solvent molecules which we refer as nanoimpurities. The impurities that are chemically distinct from the solute or solvent could be molecular (solvated) or colloidal impurities, a distinct solid phase, such as colloidal organic or inorganic nanoparticles coming from the manufacturing process of the solute or solvent. We also speculate that solute and solvent molecules could be gathered around nanoimpurities due to favorable interactions forming hybrid particles. Yet identifying the exact origin and chemical nature of these impurities is experimentally challenging[35] and not the focus of this study. Control samples, not exposed to laser pulses, showed minimal nucleation, corroborating unpublished observations by Ward[27] and Liu.[14] Doping with gold nanoparticles increased the nucleation probability to 73% postlaser irradiation, compared to 12% in control samples. This observation is consistent with NPLIN studies on ammonium

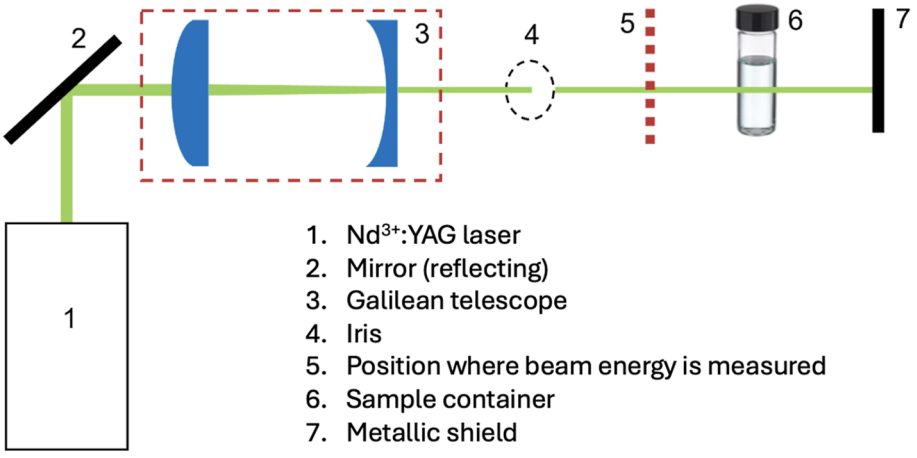

Figure 1. A schematic of the experimental setup.

https://doi.org/10.1021/acs.cgd.5c01080
Cryst. Growth Des. 2026, 26, 144−154

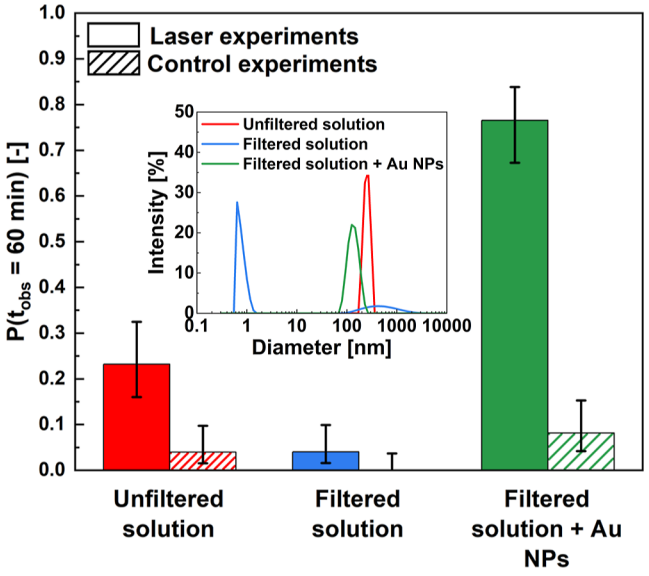

Figure 2. Effect of filtration and doping. (A) Comparison of nucleation probabilities for unfiltered, filtered and filtered solutions with the addition of AuNPs (50 nm, size specified by the manufacturer) under S = 1.5 at 25 °C. Experiments are done in two ways: unexposed (control experiments) & NPLIN (laser experiments). NPLIN experiments are conducted at a laser wavelength (532 nm) and laser peak intensity (376 MW/cm^2). The inset figure shows the particle size distributions of nanoparticles present in unfiltered, filtered and AuNP doped solutions (added concentration of 6.8 × 10^8 NPs/ml), measured by dynamic light scattering. The error bars are computed using the Wilson score method. The filter pore size is 0.22 μm. Each data point consists of 100 samples.

chloride and potassium chloride solutions,[9,27] supporting the hypothesis that nanoparticles may enhance the nucleation probability in NPLIN studies.

To explain these experimental results presented in Figure 2, dynamic light scattering (DLS) measurements were conducted to estimate the particle size distributions (PSD) in the urea solutions, as shown in Figure 2B. Measurements were conducted on unfiltered urea solutions, filtered urea solutions, and urea solutions doped with AuNPs. The PSD curve of the unfiltered urea solution revealed a dominant peak at 260 ± 40 nm, likely due to nanosized impurities or solute clusters. Filtration almost completely removed the impurities or clusters at 260 ± 40 nm from the solution, leaving only a residual population peak at diameters smaller than 1 nm. Also a significant decrease in scattered intensity upon filtration was observed. Similar observations have been reported for filtered solutions of KCl and NH_4Cl, where particle populations were also ≤1 nm, attributed to the scattering of solute molecules rather than actual particles in solution.[9,27] On the contrary, the filtered urea solution doped with 50 nm AuNPs (denoted as d_m) exhibited a population size of approximately 120 ± 20 nm, indicative of the hydrodynamic diameter (d_h). This measurement suggests that the gold nanoparticles are slightly agglomerated within the solution. Despite extensive efforts to optimize the dispersion of AuNPs within the urea solution, the level of dispersion achieved in our experiments represents the best possible outcome under the given experimental conditions. For our analysis, the AuNPs size provided by the manufacturer is considered. This assumption must be revisited when interpreting the results of our study, as the geometry and stability agglomerated nanoparticles could differ from that of well-dispersed, individual nanoparticles.

The increase in nucleation probability of (doped) solutions can be attributed to the high light absorption of gold nanoparticles. This light absorption may then lead to heating and evaporation of the local water, which is vital in the hypothesized mechanism of solute concentration due to water evaporation. See Section 4.2 for estimates of the water evaporation due to interactions of AuNPs with the laser pulse.

3.2. Effect of Laser Intensity on NPLIN. Figure 3 shows the nucleation probability of filtered urea samples containing

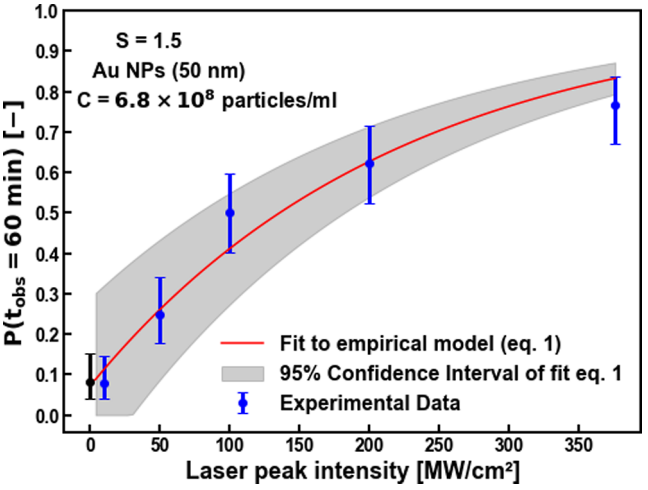

Figure 3. Nucleation probability at fixed time lag of filtered urea solution doped with AuNPs (50 nm) under different laser intensities. The particle concentration in urea solution is 6.8 × 10^8 NPs/ml. Error bars are computed using the Wilson's score method. Each data point consists of 100 samples.

50 nm AuNPs (6.86 × 10^8 NPs/ml) at various laser intensities (50, 100, 200, and 376 MW/cm^2). The nucleation probabilities observed at 10 MW/cm^2 overlapped with the control experiments, which did not involve laser irradiation. However, with increasing laser intensity, nucleation probabilities also increased, reaching 73% at an intensity of 376 MW/cm^2.

This data was fitted to a Poisson type distribution equation for the nucleation probability, whose full derivation is added to the Supporting Information.

$$P(t_{obs}) = 1 - a_I e^{-m_I(I-I_0)\sigma(I-I_0)} \quad (1)$$

here a_I is a prefactor correcting for potential spontaneous nucleation, m_I is the lability essentially similar to the constant used in the work by Alexander and Camp.,[1] I and I_0 are the laser intensity and laser intensity threshold respectively, and $u(I-I_0)$ is a step function to ensure no nucleation probability is assigned for $I \leq I_0$.

This analysis allows us to express the nucleation probability, denoted as $P(t_{obs})$, as a function of laser intensity, defined by three key parameters: the intensity sensitivity factor m_I, the spontaneous nucleation factor a_I and the laser intensity threshold I_0. The intensity sensitivity factor m_I measures the degree of change in nucleation probability in response to variations in laser intensity I, while the spontaneous nucleation factor a_I refers to the baseline probability of nucleation events occurring independently of laser intensity. The laser intensity threshold extracted by fitting eq 1 to experimental data is

https://doi.org/10.1021/acs.cgd.5c01080
Cryst. Growth Des. 2026, 26, 144−154

denoted as $(I_0)_{exp}$. This experimental value refers to the minimum threshold intensity above which laser heating of nanoparticles may lead to a cavitation bubble that acts as a nucleation site for crystallization. The fitting parameters are summarized in Table 2. Matic et al.[36] observed similar threshold values of approximately 20−60 MW/cm^2 using multiple laser pulses with unfiltered urea solutions.

Table 2. Fitting Parameters for eq 1 to the Data in 3

parameter	symbol	value	units
intensity sensitivity factor	m_I	$0.0045^{+0.0024}_{-0.0024}$	cm^2/MW
spontaneous nucleation factor	a_I	$0.918^{+0.216}_{-0.216}$	
laser intensity threshold	I_0	$2.34^{+68.82}_{-2.34}$	MW/cm^2

The experimentally obtained laser intensity threshold, $(I_0)_{exp}$. is then compared with a theoretical value for the AuNPs used in this work, $(I_0)_{theo}$, obtained using eq 2.[37] The eq 2 given below is used to calculate the theoretical laser intensity threshold, $(I_0)_{theo}$ at which the nanoparticle temperature exceeds the boiling point of the surrounding liquid, leading to the formation of a vapor layer on the nanoparticle surface. This vapor layer experiences a rapid increase in pressure, resulting in the rapid expansion and subsequent formation of a cavitation bubble.[37]

$$(I_0)_{theo} = \frac{4\pi R_{np} c_l \rho_l \gamma_l T_{boil}}{r_{abs}} \quad (2)$$

where, $(I_0)_{theo}$ represents the theoretical laser intensity threshold, R_{np} = 25 × 10^{-9} m (radius of the nanoparticle), c_l = 2815.0 J/(kg·K) (specific heat of the urea solution), ρ_l = 1166.0 kg/m^3 (density of the solution), T_{boil} = 647.0 K (boiling temperature), r_{abs} = 7.92 × 10^{-15} m^2 (absorption cross section), τ_L = 7 × 10^{-9} s (pulse duration), and γ_l = 1.83 × 10^{-7} m^2/s (thermal diffusivity of the urea solution).

The theoretical laser intensity threshold of 1.54 MW/cm^2 was calculated under the assumption that only one nanoparticle, suspended in the solution, was irradiated by the laser.[37,38] This theoretical value falls within the broad range of the experimental threshold, which is approximately $2.34^{+68.82}_{-2.34}$ MW/cm^2. The observed broad variation in the experimental intensity can be explained by relatively few data points near the lower end of the intensity scale where the threshold I_0 is located. This sparsity limits the ability of the model to accurately estimate I_0 and results in larger uncertainty and a broader confidence interval. Consequently, with fewer data points close to $I = I_0$, the model has limited information to determine precisely where the nucleation probability begins to increase significantly.

3.3. Influence of Impurity Concentration and Chemical Makeup on NPLIN. Recent studies in NPLIN research, including those by Javid et al.,[39] Ward et al.,[27] Kacker et al.,[26] and Korede et al.,[9] have highlighted the crucial role of impurity nanoparticles within supersaturated solutions and their interaction with laser energy in influencing NPLIN probabilities. In light of these findings, this section investigates the effects of impurity concentration, size, and material composition on the NPLIN probabilities.

3.3.1. Nanoparticle Concentration. Figure 4A represents the nucleation probability at a fixed time lag, t_{obs}, of 60 min, $P(t = t_{obs})$, for filtered urea samples containing 50 nm AuNPs at various nanoparticle concentrations. The experiments were conducted at a laser wavelength of 532 nm and a laser peak intensity of 376 MW/cm^2. It is evident from Figure 4A that $P(t = t_{obs})$ exhibits an overall increasing trend with increasing particle concentration. At the lower end of the nanoparticle concentration range, $P(t = t_{obs})$ was comparable to that observed in control experiments. In the intermediate concentration range (1.74−5.17 × 10^9 NPs/ml), the influence of particle concentration was modest, followed by a slight increase as the concentration exceeded 6.86 × 10^8 NPs/ml. This trend is clearly not monotonic. Control experiments performed without laser irradiation demonstrated similar nucleation probabilities across the range of nanoparticle concentrations within the observation time of 60 min.

The correlation of $P(C_{NP})$ in particle concentration C_{NP} can be absorbed into the above expression by assuming that the proportionality constant m_I is somehow linearly dependent on C_{NP}. Inserting this ansatz and recondensing the equation leads to eq 3 below.

$$P(t_{obs}) = 1 - a_I e^{-m_C C} \quad (3)$$

here a_I is the spontaneous nucleation prefactor, and m_C is a new constant similar to lability m_I but then relating to the nanoparticle concentration. For now this is referred to as the

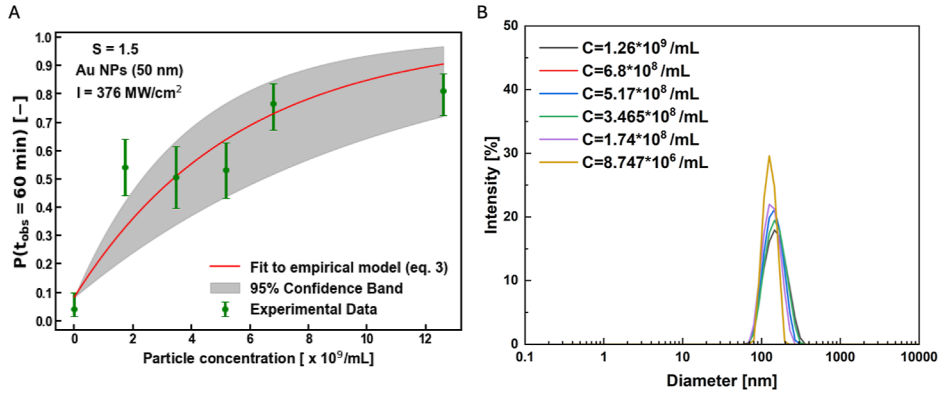

Figure 4. (A) Nucleation probability at fixed time lag of filtered urea solutions containing AuNPs (50 nm) with different nanoparticle concentration under S = 1.5 at a laser wavelength (532 nm) and laser peak intensity (376 MW/cm2) and (B) particle size distribution of filtered urea solutions containing AuNPs (50 nm) with different nanoparticle material. Error bars are computed using the Wilson's score method. Each data point consists of 100 samples.

https://doi.org/10.1021/acs.cgd.5c01080
Cryst. Growth Des. 2026, 26, 144−154

concentration sensitivity factor. See the Supporting Information for the complete derivation.

From this analysis, the equation of the fitted line describes the nucleation probability $P(t_{obs})$ as a function of nanoparticle concentration, incorporating two critical parameters: the concentration sensitivity factor m_C and the spontaneous nucleation factor a_I. Since the control experiments for filtered urea solutions doped with different nanoparticle concentrations showed similar nucleation probabilities within an observation time (t_{obs}) of 60 min (Supporting Information section 5), it can be inferred that the spontaneous nucleation rate remains relatively constant across the solutions with different nanoparticle concentrations. Consequently, a_I is obtained from the result of the curve fitting procedure of nucleation probability variation with laser intensity. The factor m_C measures the change in nucleation probability in response to varying nanoparticle concentrations. The fitting procedure yielded a concentration sensitivity factor of approximately $1.8^{+0.854}_{-0.854}\times10^{-9}$ml/particle.

The physical interpretation of the sensitivity parameter m_C remains unclear. While it is speculated that m_C may relate to an impurity heating mechanism, its precise definition within the current theoretical framework is unknown. In this context, m_C could represent the effective volume influenced by each nanoparticle through localized heating, quantifying how the energy absorbed and converted to heat by each nanoparticle affects a surrounding volume of the solution, potentially leading to crystallization via evaporation of solvent molecules. However, a rigorous theoretical formulation linking m_C to fundamental laser and solution parameters requires further investigation and lies beyond the scope of this study.

3.3.2. Nanoparticle Material. To investigate the chemical makeup of nanoparticle impurity on NPLIN probability, experiments were carried out with filtered urea samples doped with 50 nm AuNPs and 50 nm silica nanoparticles, respectively. These experiments were performed at a laser wavelength of 532 nm and a peak laser intensity of 376 MW/cm^2. Figure 5A presents the nucleation probability of these doped urea samples in comparison with control experiments. Notably, the filtered urea samples doped with silica nanoparticles showed a significantly lower nucleation probability compared to those filtered urea samples doped with AuNPs.

For filtered urea samples doped with silica nanoparticles, PSD from DLS data (Figure 5a) reveals a mean hydrodynamic diameter of 120 ± 20 nm, which is similar to that of AuNPs. This similarity in particle size between the two types of nanoparticles with distinct chemical makeup provides a consistent baseline for comparing the nucleation probabilities based on different materials. It is interesting to note that despite both nanoparticle materials supposedly being 50 nm in diameter, they both show a hydrodynamic diameter roughly 2−2.5 times this number. It is unclear whether this is due to agglomeration or something else.

Furthermore, laser irradiation enhanced the nucleation probability in the filtered urea solution doped with AuNPs relative to its control experiment. However, for the urea samples doped with silica nanoparticles, no significant difference in nucleation probability was observed when compared to their control experiment. AuNPs (50 nm), with an absorption efficiceny of 3.4, are more efficient at absorbing the 532 nm laser light than silica nanoparticles, which have an absorption coefficient of just 1.5×10^{-3}. This higher absorption coefficient leads to larger maximum size of the bubble around the AuNPs. Following the discussion given in Section 3.2, a larger maximum size of the bubble can lead to creating higher local supersaturation at the vapor−liquid interface,[18−20] which could potentially explain the higher nucleation probabilities observed in our experiments.

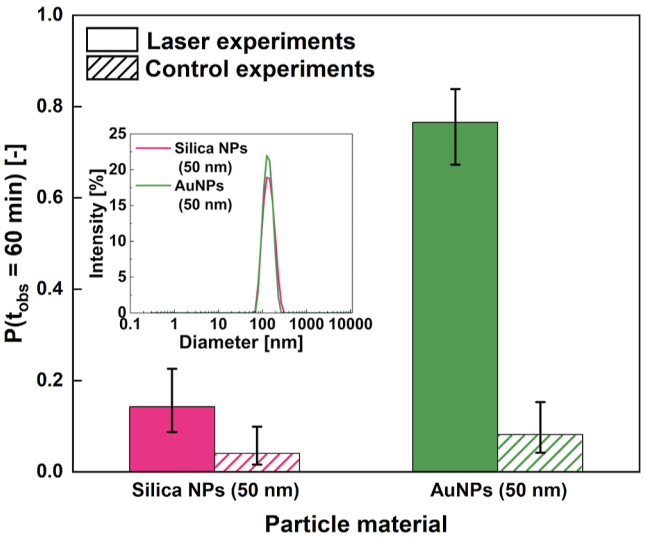

Figure 5. (A) Nucleation probabilities of doped urea solutions with different nanoparticle material under S = 1.5 at a laser wavelength (532 nm) and laser peak intensity (376 MW/cm^2) versus control (no laser exposure) experiments. The inset figure represents particle size distribution of doped urea solutions with different nanoparticle material. Error bars are computed using the Wilson's score method. Each data point consists of 100 samples.

Also, the critical laser threshold calculated using eq 2 (Supporting Information section 5) required for heating 50 nm silica nanoparticles to a degree that would induce bubble formation is significantly higher than the laser intensity used in our experiments. Therefore, for silica nanoparticles, there is effectively no bubble formation and, as a result, the nucleation probabilities observed in the filtered urea samples doped with silica overlap with those of the control experiments.

It becomes evident that impurities, which notably affect the NPLIN process, can originate from multiple sources such as the solute, the solvent, or the experimental apparatus. The experimental results presented in Figure 4, emphasizes the role of the chemical make up of nanoparticle impurities on NPLIN behavior.

Further insights into particle size distribution were obtained from dynamic light scattering (DLS) curves, as illustrated in 4B. Regardless of concentration, filtered urea solutions with AuNPs (50 nm) of different nanoparticle concentrations displayed similar size peaks at approximately 120 ± 20 nm. This consistency in particle size across varying concentrations ensures that the observed effects on nucleation probability are predominantly due to changes in nanoparticle concentration rather than particle size or other physical characteristics.

4. DISCUSSION

The previous section indicated that applying Poisson statistics and linear correlations in nanoparticle concentration and laser intensity seem to fit the data well. In this section, we try to motivate how these trends can be derived from first principles. The application of the Poisson distribution to NPLIN statistics is not new in the field,[1] therefore we believe this assumption

https://doi.org/10.1021/acs.cgd.5c01080
Cryst. Growth Des. 2026, 26, 144−154

does not require further explanation. Why exactly the linear correlations of average crystal nuclei count N_{cr} in nanoparticle concentration C_{NP} and laser intensity I work well will be discussed below.

4.1. Derivation. Our starting point for the derivation is a differential form for the average gain in crystal nuclei dN_{cr} as a function of nucleation rate J and differential volume and time dV, dt, respectively

$$dN_{cr} = JdVdt \tag{4}$$

We can obtain the total average crystal nuclei count by integrating out the volume and time elements. In principle, these integrations of the nucleation rate over space and time would be highly nontrivial. However, by virtue of the Mean Value Theorem, there must be some mean value of the nucleation rate for the NPLIN process, which we will call "J_{NPLIN}", for which the spatiotemporal integrals are constant.

The volume integration would naively be the volume carved out by a laser's path through the NPLIN experimental system (in this case, a vial). However, in the context of Impurity Heating, it is only those areas where solvent evaporation occurs that contribute to NPLIN. How we count those areas exactly is tricky: it is not the bubbles' volumes that count, but the shell volumes directly around those bubbles, and counting their exact size is somewhat arbitrary. For this section, a simplifying assumption is used that the volume of the shells is proportional to the surface area of the bubbles with a thickness δ_T, which is assumed not a function of laser intensity.

$$dV = dV_{shells} = \delta_T dA_{bubbles} \tag{5}$$

Assuming further that each nanoparticle contributes a single bubble around it and that all these bubbles have the same surface area $A_{bubble}(I)$, because we assume that they all are exposed to the same laser intensity, we can write

$$dV = A_{bubble}(I)\delta_T dN_{NP} \tag{6}$$

here $A_{bubble} = \nu(I - I_0)^{2/3}$ is assumed for some constant ν. We motivate this assumption in the next section. Then, we can integrate $dN_{NP} = C_{NP}dV_{OP}$ out where V_{OP} is the volume traced in the wake of the laser's optical path. The time integration then should simply be proportional to the lifetime of the bubbles, which is a function of laser intensity if Rayleigh-Plesset dynamics apply,[40] $\tau_{bubble} = \psi(I - I_0)^{1/3}$. With these two integrations, we obtain

$$N_{cr} = \delta_T \psi \nu J_{NPLIN}(I - I_0) I C_{NP} V_{OP} \tag{7}$$

This equation shows linear trends in both nanoparticle concentration and laser irradiated volume. Regarding the latter, this linear trend was observed empirically in recent work by Korede et al.[41] If the nucleation rate J_{NPLIN} were not a function of laser intensity, the linear trend in laser intensity is also reproduced via the combination of bubble surface area and lifetime dependency on laser intensity.

We note that the derivation above yields scalings similar to those obtained by Ndukwe-Ajala et al.[18]

4.2. Limitations of Equation 7. In the previous section, a function was derived that would explain the observed trends in nucleation statistics. However, for the linear trend in laser intensity, it was required to assume that the nucleation rate J_{NPLIN} does not depend on laser intensity, which seems implausible. According to simulations by Hidman et al.[20] and Nagalingam et al.,[19] a laser pulse would lead to increased local supersaturation proportional to laser energy supplied. The nucleation rate J is a nonlinear, monotonically increasing function in supersaturation. Therefore, J_{NPLIN} should be a monotonically increasing function in laser intensity I supplied, and likely a highly nonlinear one. The exact form of this function is very hard to estimate. It is interesting to note that this presumed nonlinear dependence is not needed to explain the data patterns observed in the literature(CITE) and in Figure 3. In one of the possible functional forms, $J = Ae^{-B/\ln^2(S)}$ with prefactor A and thermodynamic factor B. At high supersaturations, J reaches a horizontal asymptote, effectively becoming a constant in supersaturation and thereby possibly laser intensity. If the supersaturation reached during the cavitation event is sufficiently high, this might be the reason for the missing nonlinear trend. However, it could also simply be an artifact of low statistics, in which case many data points with many repetitions would show a more complex relationship between N_{cr} and I.

Another limitation of the derived model lies in the assumption that the total number of nanoparticles illuminated with laser light increases with increasing nanoparticle concentration. According to the data sheet supplied by the manufacturer for the AuNPs, the extinction constant $\epsilon = 1.72 \times 10^{-10}$ M^{-1} cm^{-1}.[42] Based on Beer–Lambert law type calculations, the laser intensity would rapidly drop below the threshold value upon entering the vial solution. This extinction length is proportional to $1/C_{NP}$, which would lead to the conclusion that the number of nanoparticles irradiated with laser light is constant for the range of concentrations studied here. In that case, the concentration dependency should not be observable. Why we then do observe such a dependency sadly remains a matter of speculation, and is a limitation of our study. We conjecture briefly in the next section about whether individual bubble events created upon laser irradiation can interact: in the above derivation it is assumed that there is no such interaction and that all thermocavitation events are isolated. We estimate the bubble size in our experiments in the next section and discuss implications there.

Another criticism that could be applied to this model is the assumption of a homogeneous distribution of AuNPs throughout the system. We do not explicitly know for instance whether the particles have a tendency to stick to the walls. Yet we can conjecture that in vial-based NPLIN experiments, that would imply that most NPLIN is observed close to the walls, which is a testable hypothesis for later works.

In summary, we have reproduced from theory the experimentally observed trends of nucleation probability in laser intensity, nanoparticle concentration, and laser-exposed volume. However, there are certain key assumptions involved in this derivation which are open to discussion. It is left outside the scope of this article how these problems are to be resolved.

4.3. Thermodynamic Model of Thermocavitation, Adjacency of Bubbles, and Implications. In the previous section, it is used that the radius of conjectured thermocavitation bubbles is proportional to $I^{1/3}$. Furthermore, there might be doubts as to whether these bubbles are proximal enough to interact. In the context of Nanoparticle Heating, we can estimate the size of bubbles formed directly from the laser energy, as illustrated in Figure 6, and relate this to the above-mentioned two points. The analytical approach adopted here follows the method outlined by Ndukwe-Ajala et al.[18] A core assumption in this analysis is that the thermal heating of water

https://doi.org/10.1021/acs.cgd.5c01080
Cryst. Growth Des. 2026, 26, 144−154

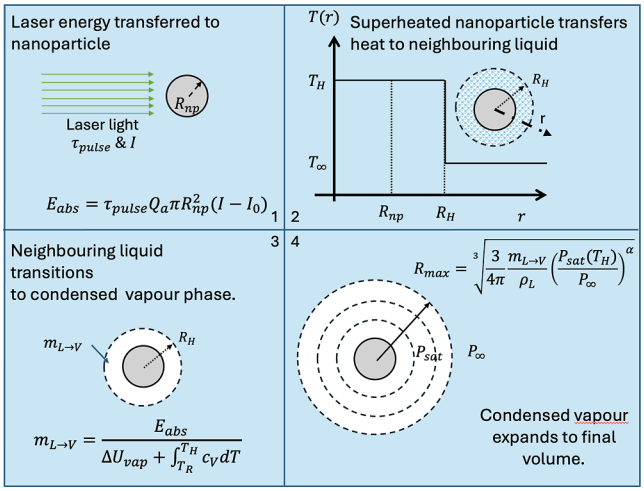

Figure 6. Thermocavitation process due to laser heating. (1): a fully immersed nanoparticle is heated by incoming laser light. (2): the hot nanoparticle transfers thermal energy to the surrounding fluid layer. (3): the now-superheated fluid turns into a hyperdense vapor phase with radius R_H determined by the mass $m_{L\to V}$. The pressure of the hyperdense vapor phase is $P_{sat}(T_H)$ where T_H is the temperature of the hyperdense vapor phase. (4): the hyperdense vapor phase expands to a maximum bubble size, R_{max}, where the internal and external pressures match.

and the subsequent expansion of the cavitation bubble are decoupled processes. This allows us to model thermocavitation as a sequence of thermodynamic equilibrium stages, significantly simplifying what would otherwise be a highly complex and computationally expensive multiphysics problem.

In the Rayleigh scattering regime ($R_{np} \ll \lambda_{laser}$), the energy absorbed ($E_{abs}$) by an isolated spherical nanoparticle of radius R_{np} is given by

$$E_{abs} = \tau_{pulse} Q_{abs} \pi R_{np}^2 (I - I_0) \tag{8}$$

where $Q_{abs} \approx 3.4$ (see the Supporting Information) is the absorption efficiency accounting for the effective cross-section (derived from Mie Scattering Theory), I_0 is the threshold intensity set at 1 MW/cm^2 here, and $\tau_{pulse} = 7$ ns is the laser pulse duration.

Neglecting radiative losses, this absorbed energy is distributed within the surrounding liquid. If we assume that the superheated region forms a homogeneous layer, the vaporized mass ($m_{L\to V}$) can be determined by assuming the final temperature of the liquid reaches $T_H = 0.8 T_{spinodal} \approx 520$ K. According to Ndukwe-Ajala et al.,[18] at this temperature, the liquid undergoes explosive expansion, initiating cavitation. Under these conditions, and assuming constant volume during heating, the vaporized mass of liquid is given by

$$m_{L\to V} = \frac{E_{abs}}{\Delta U_{vap} + \int_{T_R}^{T_H} c_V dT} \tag{9}$$

where c_V and ΔU_{vap} represent the specific heat capacity and internal energy change due to vaporization, respectively, reflecting the assumption of isochoric heat transfer. ΔU_{vap} is estimated here by $\Delta H_{vap} - R_g T_H$ where $R_g = R/M_{H_2O}$ is the specific gas constant for water.

Once formed, the new vapor mass exerts a high internal pressure against the surrounding liquid, estimated as $P_{sat}(0.8 T_{spinodal}) = 36.32$ bar.[43] Neglecting inertial effects, the bubble will expand until the internal pressure equilibrates with the surrounding liquid pressure, assumed to be 1 atm. This expansion may involve heat transfer to the surrounding liquid, but a detailed coupled heat-momentum solution is beyond the scope of this work. Instead, we consider two limiting cases: isothermal expansion ($\alpha = 1$) and adiabatic expansion ($\alpha = \gamma$, where $\gamma = 4/3$ for an ideal gas). In both cases, the bubble follows the relation

$$P_i V_i^\alpha = P_f V_f^\alpha \tag{10}$$

where P_i and V_i are the initial pressure and volume, and P_f and V_f are their final equilibrium values. Assuming the initial bubble volume is determined by the liquid phase density, the final bubble radius R_{max} is given by

$$R_{max} = \sqrt[3]{\frac{3}{4\pi} \cdot \left(\frac{m_{L\to V}}{\rho_L}\right)\left(\frac{P_c}{P_\infty}\right)^\alpha} \tag{11}$$

This expression reproduces the scaling of R_{max} with $(I - I_0)^{1/3}$ used in the previous sections since $m_{L\to V}$ scales with E_{abs} which in turn scales with $I - I_0$. Applying this expression, we estimate bubble radii of 0.65 μm for adiabatic expansion and 0.87 μm for isothermal expansion. In Ndukwe-Ajala's work[18] they estimated bubbles of size 43 nm,[18] significantly lower than what we predict. This is in line with our expectation, as both the Q_a (0.05[18] vs 3.4 in this study) value and the particle size (15 nm[18] vs 50 nm in this study) in their study are smaller resulting less energy absorbed.

To give more meaning to this predicted bubble size, the expected mean distance between nanoparticles, which serves as an estimate for the spacing between bubble nucleation sites, is given by $(C_{NP})^{-1/3}$. For a nanoparticle concentration of $C_{NP} = 6.8 \times 10^8$ particles per mL, this distance is approximately 11.3 μm. The estimated bubble to bubble spacing is in the range of 9–11 μm, which is roughly 10 to 15 times the individual bubble size at the studied AuNP concentration range.

The proximity of thermocavitation events raises questions about possible bubble–bubble interactions. The initial expansion exerts a high pressure (estimated as 36.32 bar) at the liquid–vapor boundary. Assuming negligible viscous losses, the pressure wave would be attenuated by a factor of 10^2 before reaching the next bubble, reducing the impact to 0.377 bar gauge pressure. This additional pressure is unlikely to significantly alter the final bubble size but may influence postnucleation processes near the bubble interfaces, such as attrition and breakage. Another conjecture one may draw connected to proximity of thermocavitation events is the emergence of shockwaves. The shockwaves from bubble collapse could potentially induce collisions between nanoparticles, which might alter their properties, possibly through AuNP fragmentation. If fragments are produced, they might act as additional nucleation sites for solute crystallization.

In this thermodynamic thermocavitation model, we assume that the bubbles form perfectly spherically around the colloidal impurity which absorbs the laser light for symmetry arguments. However, the impurity catches laser light first on only one side of it is body, which may lead to an asymmetrical expansion. An asymmetrical cavitation mechanism might lead to significant displacement of the colloidal impurities, which could then lead to interactions with other impurities and potential fragmentation. Particle size distribution experiments on the colloidal impurities in vials after exposure to laser lights were outside the

https://doi.org/10.1021/acs.cgd.5c01080
Cryst. Growth Des. 2026, 26, 144–154

scope of this article, so this remains a conjecture on our side. Moreover, even if these experiments were done, detecting a single fragmentation event of a nanoparticle in a large population would be extremely difficult.

While the Nanoparticle Heating model provides a simple framework for understanding NPLIN, the actual physical processes at play are likely far more complex. The assumptions of thermal equilibrium based cavitation and independent bubble expansion provide a useful first approximation but do not fully capture potential effects such as shockwave interactions, nanoparticle fragmentation, or directional bubble growth. The inherently multi scale nature of this problem suggests that additional experimental and computational investigations are needed to refine our understanding of laser induced nucleation at the nanoscale.

5. CONCLUSIONS

This study examined how experimental parameters—solution filtration, laser intensity, and impurity nanoparticle properties (concentration, composition)—affect NPLIN probability in supersaturated aqueous urea solutions. Filtration reduced NPLIN probability, while doping with AuNPs significantly increased it, underscoring the crucial role of insoluble impurities in the process, consistent with prior findings. NPLIN probability rose with both laser peak intensity and nanoparticle concentration, and seem to adhere to very similar empirical laws mathematically-this last observation has not been previously reported. Doping with different nanoparticles revealed that AuNPs yielded higher nucleation probabilities than silica nanoparticles of similar size, attributed to their greater absorption coefficients. NPLIN probability followed a Poisson distribution with respect to both nanoparticle concentration and laser intensity. To explain these trends, we propose a phenomenological model linking together these observations, based on the counting of thermocavitation events happening after laser irradiation of solution. Although the model aligns well qualitatively with experimental data, there are key assumptions involved in this model that remain open to discussion. Furthermore, our analysis of thermocavitation suggests that bubbles are within interacting range of each other, and that there is more complex physics to be investigated regarding the NPLIN mechanism. These findings may inform design of tailored impurities for NPLIN.

■ ASSOCIATED CONTENT

Supporting Information

The Supporting Information is available free of charge at https://pubs.acs.org/doi/10.1021/acs.cgd.5c01080.

PEGylation of AuNPs, TEM Images, Comparative Analysis of Nanoparticle Absorption Efficiencies at 532 nm Using Mie Theory, Control Experiments Data Across Different Concentrations of AuNPs, Critical Laser Threshold of Silica Nanoparticles, Derivation of Curve Fitting Equations 1 and 3, Sensitivity Analysis of thermocavitation model to effective maximum temperature (PDF)

■ AUTHOR INFORMATION

Corresponding Author

Hüseyin Burak Eral − *Process & Energy Department, Delft University of Technology, 2628 CB Delft, The Netherlands;* orcid.org/0000-0003-3193-452X; Email: h.b.eral@tudelft.nl

Authors

Pingping Cui − *Process & Energy Department, Delft University of Technology, 2628 CB Delft, The Netherlands; School of Chemical Engineering and Technology, Tianjin University, Tianjin 300072, People's Republic of China*

Vikram Korede − *Process & Energy Department, Delft University of Technology, 2628 CB Delft, The Netherlands;* orcid.org/0000-0002-6276-3789

Rohan P. Y. van Tooren − *Process & Energy Department, Delft University of Technology, 2628 CB Delft, The Netherlands;* orcid.org/0009-0007-6894-2490

Nagaraj Nagalingam − *Process & Energy Department, Delft University of Technology, 2628 CB Delft, The Netherlands;* orcid.org/0000-0003-4497-3691

Runze Wang − *Applied Radiation and Isotopes, Department of Radiation Science and Technology, Faculty of Applied Sciences, Delft University of Technology, Delft 2629, The Netherlands;* orcid.org/0000-0002-0542-3980

Qiuxiang Yin − *School of Chemical Engineering and Technology, Tianjin University, Tianjin 300072, People's Republic of China;* orcid.org/0000-0001-8812-0848

Antoine E. D. M. van der Heijden − *Process & Energy Department, Delft University of Technology, 2628 CB Delft, The Netherlands;* orcid.org/0000-0002-8502-8007

Herman J. M. Kramer − *Process & Energy Department, Delft University of Technology, 2628 CB Delft, The Netherlands;* orcid.org/0000-0003-3580-8432

Complete contact information is available at: https://pubs.acs.org/10.1021/acs.cgd.5c01080

Author Contributions

‖P. C., V. K. and R. P. Y. T. denotes equal contribution.

Notes

The authors declare no competing financial interest.

■ ACKNOWLEDGMENTS

This work was funded through the Open Technology Programme by Netherlands Science Foundation (NWO), project number 16714 (LightX). The authors thank the members of LightX user committee for their productive discussions; Dr. Jörn Gebauer (Bayer AG), Dr. Jana Sonnenschein (Bayer AG), Dr. Bart Zwijnenburg (Nobian B.V.), Dr. Rob Geertman (Janssen Pharmaceutica), Dr. Andreas Sieber (Lonza Group), Ir. John Nijenhuis (TU Delft). The opinions expressed in this document reflect only the author's view. The European Commission is not responsible for any use that may be made of the information it contains. P.C. thanks the China Scholarship Council (CSC) for their help and support.

■ REFERENCES

(1) Alexander, A. J.; Camp, P. J. Non-photochemical laser-induced nucleation. *J. Chem. Phys.* **2019**, *150*, 040901.

(2) Liao, Z.; Wynne, K. A Metastable Amorphous Intermediate Is Responsible for Laser-Induced Nucleation of Glycine. *J. Am. Chem. Soc.* **2022**, *144*, 6727−6733.

(3) Garetz, B. A.; Hartman, R. L. 25+ Years of Research on Nonphotochemical Laser-Induced Nucleation (NPLIN). *Cryst. Growth Des.* **2025**, *25*, 2756−2763.

(4) Garetz, B. A.; Aber, J. E.; Goddard, N. L.; Young, R. G.; Myerson, A. S. Nonphotochemical, Polarization-Dependent, Laser-Induced Nucleation in Supersaturated Aqueous Urea Solutions. *Phys. Rev. Lett.* **1996**, *77*, 3475−3476.
(5) Li, W.; Ikni, A.; Scouflaire, P.; Shi, X.; El Hassan, N.; Gémeiner, P.; Gillet, J.-M.; Spasojević-de Biré, A. Non-Photochemical Laser-Induced Nucleation of Sulfathiazole in a Water/Ethanol Mixture. *Cryst. Growth Des.* **2016**, *16*, 2514−2526.
(6) Mellah, D.; Nicolaï, B.; Fournier, B.; Bošnjaković-Pavlović, N.; Legrand, F.-X.; Gemeiner, P.; Boemare, V.; Guiblin, N.; Assi, A.; Tfayli, A.; Konate, S.; Durand, P.; Spasojević-de Biré, A. New Cocrystallization Method: Non-photochemical Laser-Induced Nucleation of a Cocrystal of Caffeine−Gallic Acid in Water. *Cryst. Growth Des.* **2022**, *22*, 5982−5995.
(7) Korede, V.; Nagalingam, N.; Penha, F. M.; van der Linden, N.; Padding, J. T.; Hartkamp, R.; Eral, H. B. A Review of Laser-Induced Crystallization from Solution. *Cryst. Growth Des.* **2023**, *23*, 3873−3916.
(8) Hua, T.; Valentín-Valentín, C.; Gowayed, O.; Lee, S.; Garetz, B. A.; Hartman, R. L. Microfluidic Laser-Induced Nucleation of Supersaturated Aqueous Glycine Solutions. *Cryst. Growth Des.* **2020**, *20*, 6502−6509.
(9) Korede, V.; Penha, F. M.; de Munck, V.; Stam, L.; Dubbelman, T.; Nagalingam, N.; Gutta, M.; Cui, P.; Irimia, D.; van der Heijden, A. E. D. M.; et al. Design and Validation of a Droplet-based Microfluidic System To Study Non-Photochemical Laser-Induced Nucleation of Potassium Chloride Solutions. *Cryst. Growth Des.* **2023**, *23*, 6067−6080.
(10) Clair, B.; Ikni, A.; Li, W.; Scouflaire, P.; Quemener, V.; Spasojević-de Biré, A. A new experimental setup for high-throughput controlled non-photochemical laser-induced nucleation: application to glycine crystallization. *J. Appl. Crystallogr.* **2014**, *47*, 1252−1260.
(11) Irimia, D.; Jose Shirley, J.; Garg, A. S.; Nijland, D. P.; van der Heijden, A. E. D. M.; Kramer, H. J. M.; Eral, H. B. Influence of Laser Parameters and Experimental Conditions on Nonphotochemical Laser-Induced Nucleation of Glycine Polymorphs. *Cryst. Growth Des.* **2021**, *21*, 631−641.
(12) Barber, E. R.; Ward, M. R.; Ward, A. D.; Alexander, A. J. Laser-induced nucleation promotes crystal growth of anhydrous sodium bromide. *CrystEngComm* **2021**, *23*, 8451−8461.
(13) Sun, X.; Garetz, B. A.; Myerson, A. S. Supersaturation and Polarization Dependence of Polymorph Control in the Non-photochemical Laser-Induced Nucleation (NPLIN) of Aqueous Glycine Solutions. *Cryst. Growth Des.* **2006**, *6*, 684−689.
(14) Liu, Y.; Ward, M. R.; Alexander, A. J. Polarization independence of laser-induced nucleation in supersaturated aqueous urea solutions. *Phys. Chem. Chem. Phys.* **2017**, *19*, 3464−3467.
(15) Takahashi, H.; Takaoka, Y.; Ebihara, S.; Tsuri, Y.; Maruyama, M.; Yoshimura, M.; Mori, Y.; Yoshikawa, H. Y. Pseudopolymorphism of Sodium Acetate in Supersaturated Aqueous Solution Induced by Focused Irradiation with Ultrashort Laser Pulses. *J. Phys. Chem. C* **2024**, *128*, 11046−11053.
(16) Takahashi, H.; Yoshikawa, H. Y.; Sugiyama, T. Exclusive and Accelerated -to- Polymorphic Transition in Glycine Crystals Induced by Femtosecond Laser Pulses. *Cryst. Growth Des.* **2024**, *24*, 10032−10037Cl.
(17) Barber, E. R.; Alexander, A. J. High-speed imaging of non-photochemical laser-induced nucleation in aqueous cesium chloride. *Phys. Chem. Chem. Phys.* **2025**, *27*, 6288−6298.
(18) Ndukwe-Ajala, K. F.; Sabirin, J. M.; Garetz, B. A.; Hartman, R. L. Microfluidic Laser-Induced Nucleation of Iron (II, III) Oxide Nanoparticle-Doped Supersaturated Aqueous KCl Solutions. *Cryst. Growth Des.* **2024**, *24*, 8370−8380.
(19) Nagalingam, N.; Raghunathan, A.; Korede, V.; Poelma, C.; Smith, C. S.; Hartkamp, R.; Padding, J. T.; Eral, H. B. Laser-Induced Cavitation for Controlling Crystallization from Solution. *Phys. Rev. Lett.* **2023**, *131*, 124001.
(20) Hidman, N.; Sardina, G.; Maggiolo, D.; Ström, H.; Sasic, S. Numerical Frameworks for Laser-Induced Cavitation: Is Interface Supersaturation a Plausible Primary Nucleation Mechanism? *Cryst. Growth Des.* **2020**, *20*, 7276−7290.
(21) Penha, F. M.; Gopalan, A.; Meijlink, J. C.; Ibis, F.; Eral, H. B. Selective Crystallization of d-Mannitol Polymorphs Using Surfactant Self-Assembly. *Cryst. Growth Des.* **2021**, *21*, 3928−3935.
(22) Liu, Y.; van den Berg, M. H.; Alexander, A. J. Supersaturation dependence of glycine polymorphism using laser-induced nucleation, sonocrystallization and nucleation by mechanical shock. *Phys. Chem. Chem. Phys.* **2017**, *19*, 19386−19392.
(23) Knott, B. C.; Doherty, M. F.; Peters, B. A simulation test of the optical Kerr mechanism for laser-induced nucleation. *J. Chem. Phys.* **2011**, *134*, 154501.
(24) Alexander, A. J.; Camp, P. J. Single Pulse, Single Crystal Laser-Induced Nucleation of Potassium Chloride. *Cryst. Growth Des.* **2009**, *9*, 958−963.
(25) Knott, B. C.; LaRue, J. L.; Wodtke, A. M.; Doherty, M. F.; Peters, B. Communication: Bubbles, crystals, and laser-induced nucleation. *J. Chem. Phys.* **2011**, *134*, 171102.
(26) Kacker, R.; Dhingra, S.; Irimia, D.; Ghatkesar, M. K.; Stankiewicz, A.; Kramer, H. J. M.; Eral, H. B. Multiparameter Investigation of Laser-Induced Nucleation of Supersaturated Aqueous KCl Solutions. *Cryst. Growth Des.* **2018**, *18*, 312−317.
(27) Ward, M. R.; Mackenzie, A. M.; Alexander, A. J. Role of Impurity Nanoparticles in Laser-Induced Nucleation of Ammonium Chloride. *Cryst. Growth Des.* **2016**, *16*, 6790−6796.
(28) Hidman, N.; Sardina, G.; Maggiolo, D.; Ström, H.; Sasic, S. Laser-induced vapour bubble as a means for crystal nucleation in supersaturated solutions-Formulation of a numerical framework. *Exp. Comput. Multiph. Flow* **2019**, *1*, 242−254.
(29) Soare, A.; Dijkink, R.; Pascual, M. R.; Sun, C.; Cains, P. W.; Lohse, D.; Stankiewicz, A. I.; Kramer, H. J. M. Crystal Nucleation by Laser-Induced Cavitation. *Cryst. Growth Des.* **2011**, *11*, 2311−2316.
(30) Li, S.; Xie, X.; Qiu, Q.; Liu, Y. Laser-induced nucleation of urea through the control of Insoluble Impurity. *Sci. Rep.* **2024**, *14*, 25777.
(31) Polat, S.; Eral, H. B. Effect of hyaluronic acid on the struvite crystallization: A structural, morphological, and thermal analysis study. *J. Cryst. Growth* **2022**, *592*, 126734.
(32) Ibis, F.; Yu, T. W.; Penha, F. M.; Ganguly, D.; Nuhu, M. A.; van der Heijden, A. E. D. M.; Kramer, H. J. M.; Eral, H. B. Nucleation kinetics of calcium oxalate monohydrate as a function of pH, magnesium, and osteopontin concentration quantified with droplet microfluidics. *Biomicrofluidics* **2021**, *15*, 064103.
(33) Briard, M.; Brandel, C.; Dupray, V. Strong Enhancement of Nucleation Efficiency of Aqueous Ethylenediamine Sulfate Solutions by Nonphotochemical Laser-Induced Nucleation: Investigations on the Role of Solid Impurities in the Mechanism. *Cryst. Growth Des.* **2023**, *23*, 7169−7178.
(34) Daniel, M.; Astruc, D. Gold Nanoparticles: Assembly, Supramolecular Chemistry, Quantum-Size-Related Properties, and Applications Toward Biology, Catalysis, and Nanotechnology. *J. ChemInf.* **2004**, *35*, 200416213.
(35) Hinnant, K. M.; Brown, L. C.; Daniels, G. C.; Capps, J. R.; Weise, N. K.; Giordano, B. C. Solution and foam properties of polyethylene oxide-lauryl acrylate random comb polymers and aggregation behavior with alkylpolyglycoside surfactants. *Colloids Surf., A* **2024**, *701*, 134667.
(36) Matic, J.; Sun, X.; Garetz, B. A.; Myerson, A. S. Intensity, Wavelength, and Polarization Dependence of Nonphotochemical Laser-Induced Nucleation in Supersaturated Aqueous Urea Solutions. *Cryst. Growth Des.* **2005**, *5*, 1565−1567.
(37) Brujan, E.-A. Numerical investigation on the dynamics of cavitation nanobubbles. *Microfluid. Nanofluid.* **2011**, *11*, 511−517.
(38) Egerev, S.; Ermilov, S.; Ovchinnikov, O.; Fokin, A.; Guzatov, D.; Klimov, V.; Kanavin, A.; Oraevsky, A. Acoustic signals generated by laser-irradiated metal nanoparticles. *Appl. Opt.* **2009**, *48*, C38.
(39) Javid, N.; Kendall, T.; Burns, I. S.; Sefcik, J. Filtration Suppresses Laser-Induced Nucleation of Glycine in Aqueous Solutions. *Cryst. Growth Des.* **2016**, *16*, 4196−4202.

https://doi.org/10.1021/acs.cgd.5c01080
Cryst. Growth Des. 2026, 26, 144−154

(40) Nagalingam, N. Laser-Induced Cavitation for Controlling Crystallization from Solution, Ph.D. thesis, TU Delft, 2024.
(41) Korede, V.; Veldhuis, M.; Penha, F. M.; Nagalingam, N.; Cui, P.; Van der Heijden, A. E.; Kramer, H. J.; Eral, H. B. Effect of Laser-Exposed Volume and Irradiation Position on Nonphotochemical Laser-Induced Nucleation of Potassium Chloride Solutions. *Cryst. Growth Des.* **2023**, *23*, 8163−8172.
(42) Sigma-Aldrich Gold Nanoparticles. https://www.sigmaaldrich.com/NL/en/technical-documents/technical-article/materials-science-and-engineering/biosensors-and-imaging/gold-nanoparticles, Accessed: 2025 Act, 21.
(43) Liu, C.-T.; Lindsay, Jr. W. T. Vapor pressure of deuterated water from 106 to 300. deg. *J. Chem. Eng. Data* **1970**, *15*, 510−513.

https://doi.org/10.1021/acs.cgd.5c01080
Cryst. Growth Des. 2026, 26, 144−154